Fabry-Perot Oscillations in the Thermopower of Ballistic Graphene Ribbons

George S. Kliros
Department of Electronics and Communication Engineering
Hellenic Air-Force Academy
Dekeleia GR-1010, Attica, Greece
Email:gsksma@hol.gr

Paraskevi C. Divari
Department of Physical Sciences and Applications
Hellenic Army Academy
Vari GR-16673, Attica, Greece
Email:pdivari@gmail.com

***Abstract*— The thermopower of ballistic graphene ribbons, at finite temperatures, is studied using linear response theory and the Landauer formalism. The dependence of thermopower on temperature and chemical potential is investigated and the obtained results are qualitatively in agreement with many features recently observed in thermoelectric measurements on high mobility graphene ribbons. Fabry-Perot oscillations in the thermopower of short ribbons as a function of chemical potential are revealed.**

I. Introduction

Graphene, an atomic layer of carbon atoms arranged in a two dimensional (2D) honeycomb lattice, are highly promising candidate for new semiconductor materials and devices [1]. In monolayer form, is gapless as its conical conduction and valence bands touch at two inequivalent Dirac-points where the density of states vanishes. The key property of graphene for electronic applications is the fast electronic transport expressed by its high carrier mobility. Since mono-layer graphene has no band-gap, it is not directly suitable for digital electronics, but is very promising for analog, high frequency applications [2]. Recently, mobilities approaching 200000 cm^2/V.s have been reported for ultraclean suspended graphene [3]. The transport characteristics of these experiments suggest that the samples reach the ballistic regime with respect to disorder scattering [4]. Ballistic transport in graphene makes it attractive for use as transistors [5], interconnects [6] as well as spin control devices [7]. Recently, the temperature dependence of conductivity in ballistic graphene ribbons was investigated by Müller $et.al.$ [8] using Landauer transport theory.

Thermopower has been used as a powerful tool to probe transport mechanisms in metals and semiconductors. Often the measurement of conductivity is inadequate in distinguishing among different scattering mechanisms and the thermopower can then be used as a sensitive probe of transport properties since it provides complementary information to conductivity. Recently, the thermoelectric properties of graphene sheets and ribbons have attracted experimental as well as theoretical attention. Theoretical studies on graphene thermopower use linear response theory incorporating the energy dependence of various transport scattering times [9] or atomistic simulations based on the non-equilibrium Green's function formalism [10]. Experimentally [11]–[13], the expected change of sign in the thermopower is found across the charge neutral point as the majority carriers change from electrons to holes. Away from the charge neutral region the thermopower behaves as $1/\sqrt{n}$, where n is the carrier density, and exhibits a linear temperature dependence in agreement with the semiclassical Mott's formula [14].

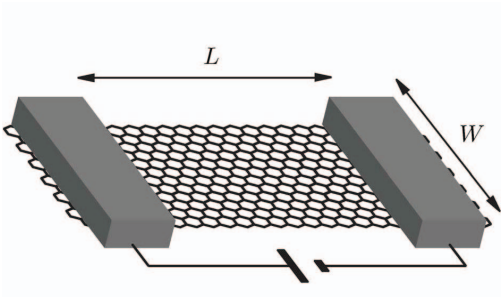

Fig. 1. Schematic of graphene ribbon of width W, contacted by two electrodes at a distance L. A voltage source drives a current through the ribbon. The chemical potential can be tuned by a separate gate electrode (not shown).

II. Thermopower of ballistic graphene

In the model for ballistic graphene proposed in Ref. [16], a nanoribbon of width W is suspended between left and right reservoirs (wide graphene regions), which are a distance L apart as shown in Fig. 1. The leads and the sample region are subject to a step-like electrostatic potential

$$\phi(x) = \begin{cases} \phi_\infty & x < 0 \quad \text{(left-lead)}, \\ 0 & 0 < x < L \quad \text{(sample)}, \\ \phi_\infty & x > L \quad \text{(right-lead)}, \end{cases} \tag{1}$$

the zero of energy being chosen as the Dirac point in the sample region. Modeling the leads by highly doped graphene, the parameter ϕ_∞ is much grater than the chemical potential and drops out of the results in the end. Ballistic transport requires the sample length L to be shorter than the mean free path of carriers ℓ. In nearly impurity free samples the mean free path is limited by inelastic scattering, dominated at low temperatures by Coulomb scattering. However, on a clean substrate with large dielectric constant or in the presence of nearby metallic contacts [4], Coulomb scattering is relatively weak and therefore the non-interacting model is applicable.

978-1-4244-7700-5/10/$26.00 ©2010 IEEE

By means of linear response theory and the Landauer formalism, the thermopower of ballistic graphene in the absence of scattering can be written as [15]

$$S = -\frac{k_B}{e}\frac{\int_0^\infty dE\big(-\frac{\partial f(E)}{\partial E}\big)\frac{E-\mu}{k_BT}\sum_{n=0}^{\infty}T_n(E)}{\int_0^\infty dE\big(-\frac{\partial f(E)}{\partial E}\big)\sum_{n=0}^{\infty}T_n(E)} \quad (2)$$

where $T_n(E)$ is the transmission probability, $f(E) = (1 + \exp[(E-\mu)/T])^{-1}$ is the Fermi distribution function and n labels the transverse modes of the graphene ribbon. Moreover, it is convenient to use for the derivative of the Fermi-Dirac function in Eq. (2) the following relationship

$$\frac{\partial f(E)}{\partial E} = -\frac{f(E)}{k_BT}\big[1 - f(E)\big] \quad (3)$$

The transmission probability $T_n(E)$ at energy E, can be obtained by solving the Dirac-electron propagation problem through the potential of Eq.(1) in the limit $|\phi_\infty| \to \infty$ that corresponds to an infinite number of propagating modes in the leads,

$$T_n(E) = \left|\frac{k_n}{k_n\cos(k_nL) + i\frac{E}{\hbar v_F}\sin(k_nL)}\right|^2, \quad (4)$$

where $k_n = (\hbar v_F)^{-1}\sqrt{E^2 - (\hbar v_F q_n)^2}$, W the width of the ribbon and $v_F \approx 10^6$ m/s is the Fermi velocity. The transverse momentum q_n is defined for various boundary conditions as $q_n = (n+\gamma)\pi/W$. Below we use $\gamma = 1/2$ corresponding to infinite mass confinement [8]. The transmission probabilities depend on the aspect ratio W/L of the graphene ribbon and also on microscopic details of its upper and lower edge. For short and wide ribbons ($W/L \gg 1$) these microscopic details become insignificant. The above continuum model has been tested by comparing with a numerical solution based on a tight-binding model on a honeycomb lattice and is found to be quite accurate [16].

III. Results and Discussion

In order to facilitate the comparison with experimental results, we show in Fig.2 the dependence of theropower S on chemical potential μ for various temperatures T, based on the full numerical evaluation of Eq. (2) for a graphene ribbon of finite width $W = 1.5\ \mu m$ and aspect ratio $W/L = 3$. Experimentally, the chemical potential of the graphene ribbon can be controlled by applying a gate voltage that will cause doping of graphene's π-bands with electrons or holes (depending on the sign of gate voltage). As is illustrated in Fig.2, the simulated S versus chemical potential μ curves are qualitatively similar to the experimental curves of Refs. [11], [13] in terms of its antisymmetric shape to the Dirac point $\mu = 0$ (middle of the bandgap) and its distinctive peak. The peak value of the simulated S is of the order of (k_B/e), close to the experimental value. However, scattering may be responsible for the different dependence of the peak values

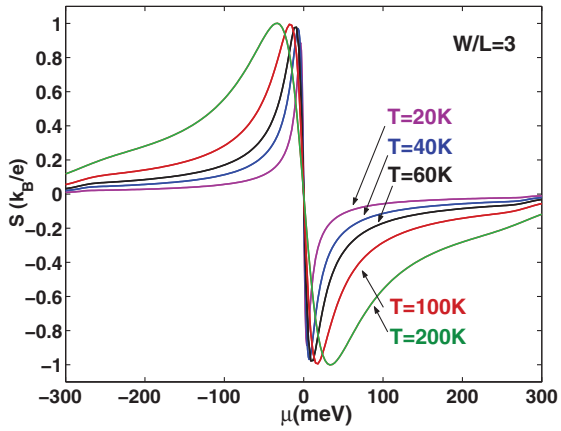

Fig. 2. Thermopower S versus chemical potential μ for various temperatures T. The aspect ratio of the ribbon is $W/L = 3$.

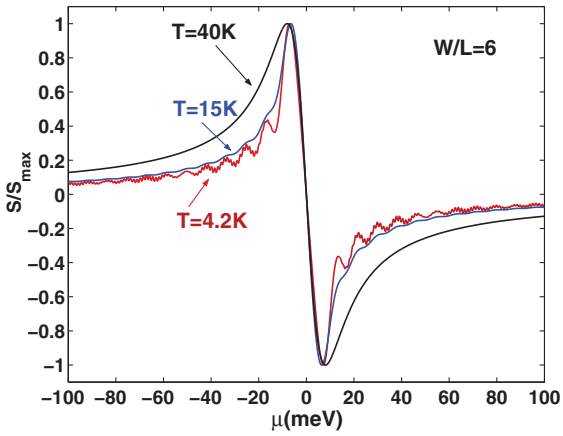

Fig. 3. Oscillating thermopower S versus chemical potential at low temperatures $T = 4.2K, 15K$ and $40K$, for a ribbon with aspect ratio $W/L = 6$.

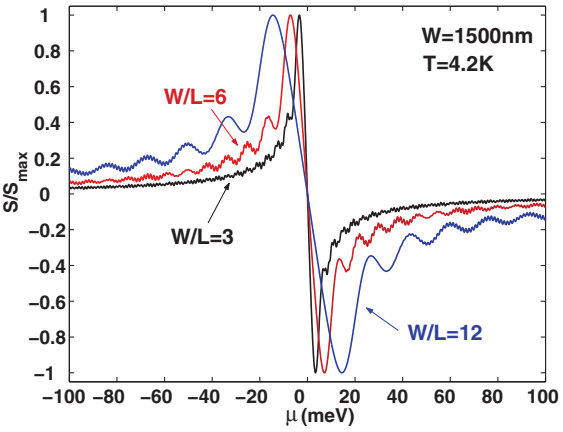

Fig. 4. Normalized thermopower S/S_{max} versus chemical potential for various aspect ratios at $T = 4.2K$

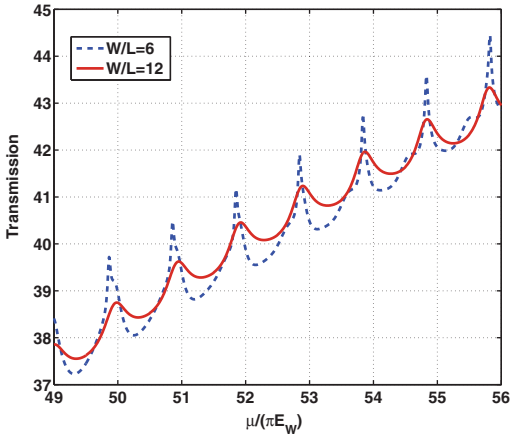

Fig. 5. Total Transmission versus chemical potential for aspect ratios of the ribbon $W/L = 6$ and $W/L = 12$.

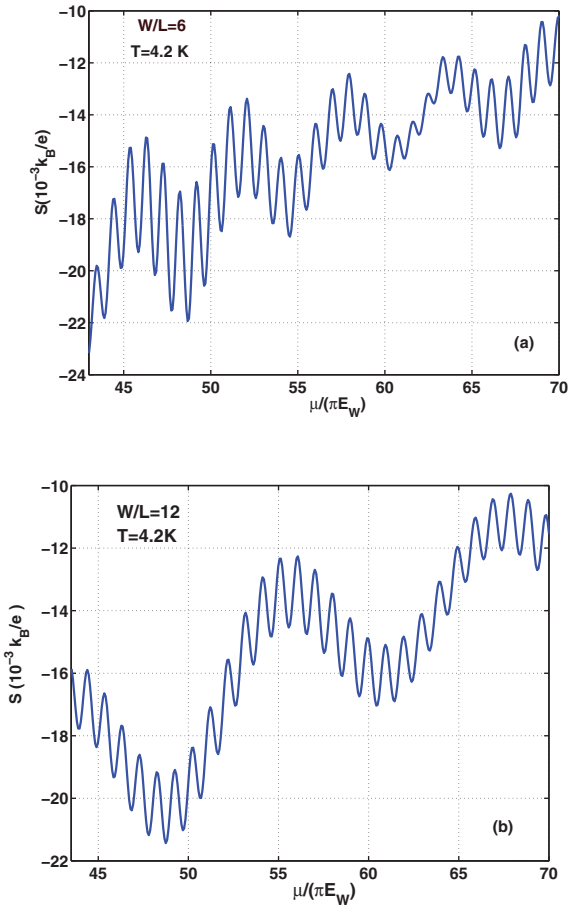

Fig. 6. (color online) Fabry-Perot resonances in thermopower S of a very short graphene ribbon with (a)$(W/L = 6)$ and (b) $(W/L = 12)$ at low temperature $T = 4.2K$.

on temperature in the experiment. Moreover, all curves have maximum when the chemical potential is several k_BT away from the middle of the bandgap.

In Fig.3 the normalized thermopower (to its maximum) S/S_{max} versus chemical potential is plotted in the low-temperature regime for a ribbon with aspect ratio $W/L = 6$. As temperature decreases, Fabry-Perot oscillations of decreasing amplitude with chemical potential, are revealed. Moreover, the dependence of these oscillations on the aspect ratio of the ribbon is illustrated in Fig.4. As is shown, for a short and wide sample, there are two kinds of Fabry-Perot oscillations: Fast oscillations with period $(\Delta\mu)_{fast} = \pi E_W$, where $E_W \equiv \hbar v_F/W$ superposed to slow ones with period $(\Delta\mu)_{slow} = \pi E_L$, where $E_L \equiv \hbar v_F/L$. Furthermore, as is seen in Fig.4, the fast oscillations become more pronounced with growing μ, while the slow ones decrease in amplitude.

Analyzing the dependence of the transmission coefficient of Eq.(4) on the chemical potential μ, with k_n being real, i.e.,

$$T_n(\mu) = \frac{\mu^2 - (\hbar v_F q_n)^2}{\mu^2 - (\hbar v_F q_n)^2 \cos^2(k_n L)}, \tag{5}$$

we can find that Fabry-Perot resonances are expected. Fig. 5 depicts the oscillatory behavior of the total transmission for a infinite number of propagating modes in the ribbon as a function of the dimensionless parameter $\mu/\pi E_W$ for short ribbons with $W/L = 6$ and $W/L = 12$. As it is seen, oscillations with period roughly equal to πE_W are revealed with amplitude decreasing with the ratio W/L. When there is a propagating mode at the Fermi level whose longitudinal wavevector k_n is commensurate with the length of the ribbon, i.e.,

$$k_n^{(m)} = (\hbar v_F)^{-1}\sqrt{\mu^2 - (\hbar v_F q_n)^2} = \frac{m\pi}{L}, \quad m = 1, 2, \ldots \tag{6}$$

the following relation for the corresponding values of the chemical potential is obtained:

$$\frac{\mu_n^{(m)}}{\pi E_W} = \sqrt{\left(n + \frac{1}{2}\right)^2 + m^2\left(\frac{W}{L}\right)^2}. \tag{7}$$

According to Eq.(7), fast oscillations corresponding to fixed m appear with roughly periodic spacings $(\Delta\mu)_{fast} = \pi E_W$ while slow oscillations originate from modes with small transverse quantum numbers n and appear with roughly periodic spacings $(\Delta\mu)_{slow} = \pi E_L$. This is clearly depicted in Fig.6 (a) and (b) for ribbons with $W/L = 6$ and $W/L = 12$, respectively.

Concerning their physical origin, the fast oscillations come from longitudinal modes with large quantum numbers n, which enters the sample and since $W >> L$, scatter back and forth many times between the sample edges. As a consequence, these oscillations are very sensitive to edge roughness. On the other hand, slow oscillations originate from the modes with small quantum numbers n which transverse the sample in straight paths. The later oscillations are very sensitive to temperature (see Fig.3).

IV. Conclusion

We calculated the thermopower as a function of both chemical potential and temperature for different aspect ratios W/L of the graphene ribbons. Our calculations explains qualitatively most of the features observed in recent thermoelectric measurements of graphene. In short graphene ribbons, at low-temperatures, slow and fast Fabry-Perot oscillations in the thermopower versus chemical potential are demonstrated and a prediction for the corresponding periods is given. We found that these oscillations are very fragile with respect to finite temperatures as well as to aspect ratio of the ribbon. Moreover, because of their sensitivity to edge roughness and inelastic scattering, their experimental observation might prove challenging. It is worthwhile to note that the electronic and thermoelectric transport properties of narrow graphene nanoribbons are strongly dependent on the chirality of the ribbon and the continuum model fails to describe accurately the edge termination effects [17]. In this paper, we address our calculations in short and wide graphene ribbons ($W/L \geq 3$) where the microscopic details of upper and lower edge become insignificant so that the "continuum description" of graphene is valid. Its validity has been examined in previous studies [18] by comparing with a numerical solution based on a tight-binding model with armchair edges. However, we expect that the above discussed trends hold for other boundary conditions [19] at the edges of the graphene ribbons.

References

[1] A.H. Castro Neto, F. Guinea, N.M.R. Peres, K.S. Novoselov, A.K. Geim, "The electronic properties of graphene", Rev. Mod. Phys., vol.81, pp. 109-162, 2009.

[2] Z. Chen, Y. Ming Lin, M.J. Rooks, P. Avouris, "Graphene nano-ribbon electronics", Physica E Vol. 40, pp. 228-232, 2007.

[3] K.I. Bolotin, K.J. Sikes, J. Hone, H.L. Stormer, and P. Kim, "Temperature-dependent transport in suspended graphene", Phys. Rev. Lett., Vol. 101, no.9, pp. 096802(1)-(4), 2008.

[4] X. Du, I. Skachko, A. Barker, and E.Y. Andrei, "Approaching ballistic transport in suspended graphene", Nature Nanotechnology, Vol.3, pp.491-495, 2008.

[5] G. Liang, N. Neophytou, D. Nikonov, and M. Lundstrom, "Performance projections for ballistic graphene nanoribbon field-effect transistors", IEEE Trans. on Electron Devices, Vol. 54, no. 4, pp. 677-682, 2007.

[6] A. Naeemi and J. D. Meindl, "Conductance modeling for graphene nanoribbon (gnr) interconnects," IEEE Electron Device Letters, Vol. 28, no. 5, pp. 428-431, 2007.

[7] N. Tombros, C. Jozsa, M. Popinciuc, H.T. Jonkman and B.J. van Wees, "Electronic spin transport and spin precession in single graphene layers at room temperature", Nature (London), Vol. 448, pp. 571-574, 2007.

[8] M. Müller, M. Bräuninger and B. Trauzettel, "Temperature dependence of the conductivity of ballistic graphene", Phys. Rev. Lett., Vol. 103, art. no. 196801, 2009.

[9] E.H. Hwang, E. Rossi and S. Das Sarma, "Screening-induced temperature-dependent transport in two-dimensional graphene", Phys. Rev. B, Vol. 80, art. no. 165404, 2009.

[10] Y. Ouyang and J. Guo, "A theoretical study on thermoelectric properties of graphene nanoribbons", Appl. Phys. Lett., Vol. 94, art. no. 263107, 2009.

[11] Y.M. Zuev, W. Chang, and P. Kim, "Thermoelectric and magnetothermoelectric transport measurements of graphene", Phys. Rev. Lett., Vol.102, art. no. 096807, 2009.

[12] P. Wei, W.Z. Bao, Y. Pu, C.N. Lau, and J. Shi, "Anomalous thermoelectric transport of dirac particles in graphene", Phys. Rev. Lett., Vol. 102, art. no. 166808, 2009.

[13] J. Checkelsky, N. Ong, "Thermopower and Nernst effect in graphene in a magnetic field", Phys. Rev. B, Vol. 80, art. no. 081413(R), 2009.

[14] M. Cutler and N.F. Mott, "Observation of Anderson Localization in an Electron Gas", Phys. Rev. B, Vol.181, pp. 1336-1340, 1969.

[15] G.D. Guttman, E. Ben-Jacob, and D.J. Bergman, "Thermopower of meso- scopic and disordered systems", Phys. Rev. B, Vol. 51, no. 24, 17758-17766, 1995.

[16] J. Tworzydlo, B. Trauzettel, M. Titov, A. Rycerz, and C.W.J. Beenakker, "Sub-poissonian shot noise in graphene", Phys. Rev. Lett., Vol. 96, art. no. 246802, 2006.

[17] J. J. Palacios, J. Fernndez-Rossier, L. Brey and H. A. Fertig, "Electronic and magnetic structure of graphene nanoribbons", Semicond. Sci. Technol. Vol. 25, art. no. 033003, 2010.

[18] L. Brey and H. A. Fertig, "Electronic states of graphene nanoribbons studied with the Dirac equation", Phys. Rev. B, Vol.73, art. no. 235411 (2006).

[19] E. McCann and V.I. Fal'ko, "Symmetry of boundary conditions of the Dirac equation for electrons in carbon nanotubes", J. Phys. Condens. Matter, Vol. 16, pp. 2371-2379, 2004.